Engineering of Silica Thin-Film Nanoporosity via Alkali-Ion-Assisted Reconstruction

Mickael Boudot, Cédric Boissière, Ekaterina Burov, Thierry Gacoin

Engineering of Silica Thin Film Nanoporosity Via Alkali Ion Assisted Reconstruction

Mickael Boudot,*[1] Cédric Boissière,[2] Ekaterina Burov,[3] and Thierry Gacoin*[1]

[1]Laboratoire de Physique de la Matière Condensée, UMR 7643, Ecole Polytechnique, CNRS, Université Paris-Saclay, Route de Saclay, 91128 Palaiseau cedex, France.
[2]Sorbonne Université, CNRS, Collège de France, UMR 7574, Chimie de la Matière Condensée de Paris, F-75005 Paris, France.
[3]Laboratoire Surface du Verre et Interfaces, UMR 125 CNRS/Saint-Gobain, 93303 Aubervilliers, France.

Abstract:

We report a method to prepare patterned mesoporous silica-based films with a fine control of the pore sizes and the porous fraction by combining the sol gel approach with an alkali ion post-treatment. Strategy involves the porous mesostructure reconstruction of surfactant (CTAB or F127) templated silica films by alkali metal ions diffusion into the inorganic matrix at 450°C. Coatings with pores ranged from 2 nm to 100 nm, gradient of pore sizes and porous volumes as well as 2D patterned structures were obtained by optimizing the alkali ions assisted reconstruction process (alkali ions amount, liquid deposition techniques, …). Na^+, Li^+ and K^+ are demonstrated as efficient silica network modifiers to significantly and rapidly tailor the mesostructure of the film. Using spectroscopic ellipsometry, SEM, environmental ellipsometry porosimetry, atomic absorption spectroscopy, and phase diagram simulations, two different alkali ions-induced mechanisms were identified: the densification of the silica framework and the separation in two phases of the silica matrix. Both mechanisms are easily controlled separately by adjusting the process conditions and the kind of ions used. This study, with the demonstration of an adaptive multi-responsive antireflective coating, shows that alkali ions assisted pore restructuration is complementary to the existing sol gel techniques and is promising for the design of new functional smart materials.

Introduction:

Synergic coupling between liquid-phase sol gel chemistry that permits to fashion inorganic or hybrid materials in particles, thin films, monoliths, membranes *etc.*[1–4] and self-assembled amphiphilic molecule mesophases[5,6] has given birth to an important class of nanostructured materials with potential applications in various fields such as catalysis and separation, drug delivery, optics, sensing, stimuli responsive materials, and so forth.[7–13]

In such combination, micellar and lyotropic liquid-crystal phases act as a scaffold around which sol gel precursors condense, generating mesoporous materials after the elimination of the structuring agents. According to the nature of the surfactant template (divided in two main families: amphiphilic block copolymers and ionic or nonionic surfactants) and the synthesis conditions, the inorganic or hybrid porous materials can exhibit various well controlled 2D or 3D periodically ordered mesostructures (i.e. disorganized, worm-like, hexagonal and cubic symmetries) and diverse pore size distributions commonly comprised between 2 nm and tens of nanometers. For instance, cetyltrimethylammonium bromide (CTAB) is a well-known ionic surfactant forming ca. 2 nm pore sizes, while Pluronic F127 ($EO_{106}PO_{70}EO_{106}$) triblock copolymer is routinely used to reach pore sizes up to about 8 nm.[14,15]

Because of the extraordinary flexibility of silica sol gel chemistry, porous silica based materials are the object of intensive researches. Most of them concern the design of the pore network in the different classes of materials (monoliths, powders, thin film) with the objective of controlling the pore volume fraction, size and connectivity. Interesting issues also concern the development of processes leading to materials with a hierarchical porosity,[16–19] i.e. materials with a distribution of pores that are usually developed for optimizing diffusion processes. However, surfactant templated routes for these kinds of materials still suffer limitations such as the difficulty to design structures with large pores due to the intrinsic small size of most of amphiphilic molecules.

Materials with large pores are highly demanded, for instance to control/prevent nanoscale physicochemical phenomena like capillary condensation or to host and deliver large guest molecules i.e. proteins and DNA.[20–22] A common strategy involves expanding the volume of self-assembled surfactant micelles by adding, directly in the sol gel solution, nonpolar molecules or polymers called swelling agents. They accumulate into the hydrophobic cores of the mesophase and swell it, which finally results in materials with larger pores dimensions after elimination of the organic mesophase. This strategy is fruitful only for solution processings, for example in case of silica particles synthesized by precipitation or hydrothermally treated, and leads to 3 times up to 10 times larger pores.[20,23,24] A recent work by Dunphy et al. demonstrated that swelling agents have a limited impact for thin films and particles synthesized using the evaporation-induced self-assembly (EISA) method.[25,26] Authors proposed, either to mix two copolymers of similar structures or to increase surfactant/SiO_2 ratio in order to prepare by EISA porous silica thin films with pore sizes ranging from 4.5 nm to 30 nm maximum.[27] Others alternatives based on superstructures composed of amphiphilic high molecular weight copolymers like polystyrene-block-poly(ethylene oxide) were described in literature with silica thin films showing pores sizes up to 30 nm.[28,29] Unfortunately this kind of templates are complicated to manipulate due to their limited solubility in alcohols.[29,30] Moreover, they are fairly expensive and not always commercially available. Some studies demonstrated that hard templates as latex or dendrimers can substitute self-assembled templates leading to very monodisperse pore distributions and large ranges of accessible sizes .[29,31,32] In a more exotic way, Malfatti *et al.* reported on the model of EISA, formation of NaCl nanocrystals during solvent evaporation that, after removal of said nanocrystals, leaves original cubic nanobox-like pores of around 260 nm in hierarchical silica films.[33]

Despite all these efforts to develop efficient strategies to large pores, those reported up to now are still not fully satisfactory regarding either the narrow range of large pore diameter that can be designed, the simultaneous low control of the porous volume fraction or their compatibility with scale-up in terms of cost-effectiveness, feasibility, etc.

In the present work, we report on an innovative, straightforward and efficient post-treatment that allows to finely engineer the porosity of silica both regarding their porous volume fraction and the pore sizes, from few to hundreds of nanometers. We here focus on silica coatings, starting from CTAB or F127 surfactant templated films synthesized by a conventional EISA routes. The starting idea was to investigate how the addition of alkali ions associated to a thermal treatment would allow to modify the porous network. Associating sol-gel chemistry to alkaline silicate glass properties, we show that the alkali ions assisted post-reconstruction is a simple way to finely tune the pore size at a relative low temperature of 450°C, compatible to usual glass substrates. Structural and chemical transformation of films induced by Li^+, Na^+ or K^+ ions diffusion upon thermal treatment was monitored by a set of ex situ techniques such as spectroscopic ellipsometry, SEM, environmental ellipsometry porosimetry (EEP), and atomic absorption spectroscopy (AAS). The observations clearly

evidence two distinct phenomena that are controlled by alkali ions concentration in silica layer. First at low alkali ions contents, a densification mechanism takes place within the films during the diffusion of the alkali species allowing the modification of the porous volume of the thin films. Second, at high alkali ions contents, the increasing quantity of diffusing ions in silica matrix provokes phase separation mechanisms exploited to tailor morphology and size of pores between 2 nm and around 100 nm. In addition to allow the elaboration of coatings with adjustable porosities, we show that our process provides a unique opportunity for the development of coatings with patterned porosities, i.e. with areas exhibiting surface distributions of pore size and pore densities that could be selectively organized within the coating in gradient by a very simple manner using only inorganic chemistry.[34,35] Examples are given in the case of a silica mesoporous antireflective (AR) coating on glass showing an adaptable response thanks to an in-plane gradient of reflection property.

Materials and Methods:

Chemical Reactants: Absolute ethanol 100% (EtOH), 37% HCl were purchased from Carlo Erba and tetraethylorthosilicate (TEOS) ≥ 99%, Sodium acetate trihydrate ≥ 99%, Lithium Acetate dihydrate ≥ 99%, Potassium acetate ≥ 99%, hexadecyltrimethylammonium bromide ≥ 99% (CTAB), and Pluronic F127 ($EO_{106}PO_{70}EO_{106}$) were purchased from Sigma Aldrich. All products were used as received.

Film Processing: CTAB-templated mesoporous silica thin films were prepared from solutions composed of TEOS/CTAB/HCl/H_2O/EtOH with respective molar ratios of 1:0.11:0.16:4.9:23. F127-templated mesoporous silica thin films were prepared from solutions composed of TEOS/F127/HCl/H_2O/EtOH with respective molar ratios of 1:0.003:0.16:4.9:23. For both solutions, TEOS was first dissolved in EtOH, HCl (2M), and H_2O before adding the organic template. The solution was stirred for at least 8 h at room temperature and filtrated using a 0.45µm Nylon filter before use. Films were prepared on silicon wafers by spin-coating at room temperature without any atmosphere control and at constant rotating speed of 2000 rpm for 1 min. After deposition, thin films were immediately calcined at 450°C for 15 min.

Pores restructuration of mesoporous silica films was carried out using sodium acetate, lithium acetate and potassium acetate hydro-alcoholic solutions with concentrations comprised between 9.10^{-3} M and 1.5 M. Hydro-alcoholic solvent is composed of 15mL H_2O + 2 mL EtOH. Solutions were obtained by dissolving alkali metal salts in the hydro-alcoholic solvent at 90°C for few minutes to accelerate the dissolution. Salts solutions were spin coated on porous silica films at 2000 rpm at room temperature, except for sodium acetate solutions with concentrations $[Na^+] > 0.4$ M that were heated up at 90°C for 1 min before spin coating to keep the salt dissolved. After deposition, films were calcined at 450°C for 10 min, then cooled down at room temperature, washed by soaking them in deionized water at pH = 2 for 30 sec approximately, before to be rinsed with deionized water and dried with N_2. Films were labelled Na-SiO_2, Li-SiO_2 and K-SiO_2 after Na^+, Li^+ and K^+ induced restructuration.

Characterization: Spectroscopic ellipsometry analyses were performed on an UV−visible variable-angle spectroscopic ellipsometer (MM-16 Horiba Jobin Yvon) equipped with a dry atmosphere cell. Films thicknesses and refractive indexes were extracted from conventional Ψ and Δ dispersions using a Cauchy model (DeltaPsi 2 software). Ellipsometry porosimetry experiments were performed on a UV-visible variable angle spectroscopic ellipsometer (Woollam M-2000, V.A.S.E software) equipped with a humidity atmosphere cell using an Aceflow (SolGelWay) gas flow controller. Films thicknesses and refractive indexes were extracted from a single layer Cauchy model. Pore size distributions were determined from adsorption isotherms, recorded between RH = 10% and RH = 80%, using a modified

Kelvin model and assuming pores with spherical shape.[14] For lithium, sodium and potassium atomic absorption spectrometry, we used a SpectrAA 220 Varian. Scanning electron microscopy (SEM) pictures were obtained with a Hitachi S-4800. Samples were coated with platinum by sputtering to avoid accumulation of electrons. Transmittance analyses of Na-SiO_2 thin film on microscope glass were carried out on a Cary 50 spectrophotometer in normal incidence in dry atmosphere. Grazing incidence X-Ray diffraction (GIXRD) was performed using a Bruker D8 Discover diffractometer equipped with a Cu tube, a Goebel mirror, a 0.6 mm thick divergence slit, some 2.5° primary Soller slits, a plane collimator and the 0D LynxEye detector. 2Theta scans were collected with a grazing omega = 0.9° angle.

Results and Discussion:

1) Tuning Porosity of SiO_2 Thin Films Using Sodium ions.

1.1 Na-SiO_2 Thin Films Synthesis and Characterization.

Pristine sol gel mesoporous silica films with thicknesses of 280 ± 20 nm were synthesized by evaporation-induced self-assembly (EISA) method[26] using TEOS as precursor and CTAB as micellar template on silicon substrates. A thermal curing at 450°C for 15 min allows to free the porosity and to strengthen the mesoporous silica matrix (see Materials and Methods section for more details). Obtained sol gel CTAB-templated pristine silica films are composed of pores with sizes, determined by environmental ellipsometry porosimetry (EEP)[14], of about 2 nm (see S.I.1). In this work we focus on the evolution of pore sizes and porous volumes of such mesoporous films induced by the chemical activity of alkali ions on the condensed silica walls of the porous framework.

Sodium ions insertion in siliceous framework was performed by ion migration at the relative low temperature of 450°C from salt solutions spin coated on top of pristine silica films. The direct addition of a sodium salt in the sol gel solution containing the porogen and the silica precursor was not performed in this work because a water-induced phase separation phenomenon has been reported for films prepared with CTAB/Na^+/TEOS sol gel solutions.[36] Sodium acetate trihydrate was selected as sodium source due to its relatively high solubility in hydro-alcoholic solutions, which enables liquid deposition with a fairly good surface homogeneity. To obtain high concentrations ([Na^+] > 0.4M), moderate heating of solutions (60°C) was required before deposition. Moreover, the acetate organic counter ions can be eliminated by combustion at 450°C, and the potential carbonate formed at high temperature can easily be removed by a washing with an acidic aqueous solution. Experimentally, sodium acetate solutions, with concentrations of 0.01/0.02/0.07/0.21/0.41/0.63/0.83 and 1.04 M, were spin coated onto pristine porous SiO_2 layers. After salt deposition, films were annealed at 450°C for 10 min, washed with pH = 2 (HCl) deionized water and rinsed with deionized water to remove the excess of salt and finally dried. Process of alkali ions insertion into porous silica is schematically described in the Supplementary Information (S.I.2). In following text, samples are characterized and labeled using their initial Na/Si ratio, referred to as the initial relative amount of alkali and silica before the annealing and washing treatments.

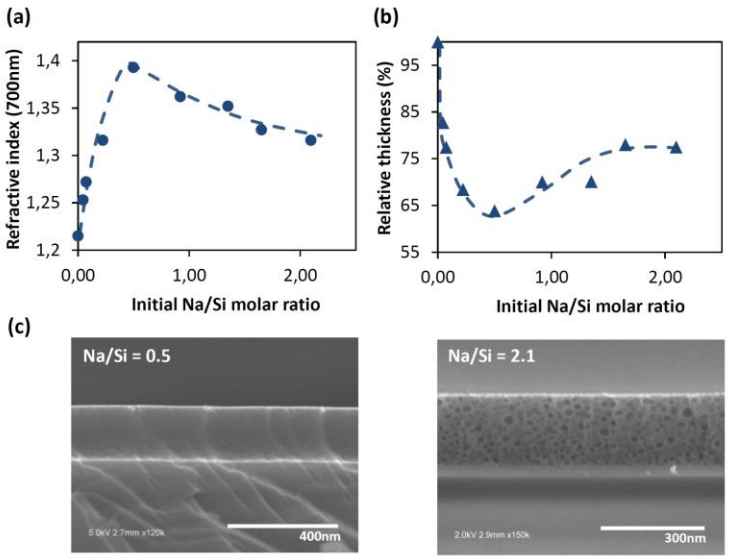

Figure 1. (a) Refractive index and (b) relative thickness of Na-SiO_2 films depending on the initial Na/Si molar ratios.(c) Cross section SEM images of Na-SiO_2 films obtained with the initial molar ratios Na/Si = 0.5 and Na/Si = 2.1.

In Figure 1a and 1b, refractive indexes and thicknesses of sodium-modified silica films (Na-SiO_2) obtained by spectroscopic ellipsometry analyses are reported for various initial Na/Si molar ratios. Initial molar ratios are determined from initial molar amount of sodium (measured by atomic absorption spectroscopy in re-dissolving, in water and before the 450°C treatment, the sodium acetate deposited by spin coating) and silica (estimated by ellipsometry measurements using Bruggeman effective medium approximation[37]) on the top of each samples before thermal treatment and washing. Two distinct parts are clearly visible for both thickness and refractive index plots. First, for low initial sodium amounts comprised between Na/Si = 0 and Na/Si = 0.5, Na-SiO_2 films refractive index values increase from n_{700} = 1.22, for pristine mesoporous silica, to a maximum value for Na/Si = 0.5 around n_{700} = 1.39. This rise of refractive index is concomitant to a drastic decrease of film thicknesses. As an example, film thickness of Na/Si = 0.5 film thickness is reduced by 36% compared to Na/Si = 0. In parallel, cross section SEM image of Na-SiO_2 film for Na/Si = 0.5 (see Figure 1c) reveals, despite strong refractive index and thickness changes, that Na-SiO_2 layers keep their mechanical integrity without any evidences of a structure collapse. This proves with certainty that mesoporous silica layers undergo a phenomenon of densification.[38] Similar observations have been already reported in case of porous TiO_2 films deposited onto glass substrate from which alkaline or alkaline earth ions can migrate into the top porous layer during thermal annealing.[39,40] Using the Bruggeman effective medium approximation and the refractive indexes of inorganic matrixes of Na-SiO_2 films determined by EEP for a humidity of 0%, thin film porous volumes were calculated depending on the initial Na/Si ratios. Porous volume values of 48%, 35% and 11%, for pristine porous silica, Na-SiO_2 (Na/Si = 0.07) and Na-SiO_2 (Na/Si = 0.5) thin films have been obtained respectively. Such porous fraction evolution highlights that the higher is the initial amount of salt, the higher is the loss of porosity during sodium thermal migration. It is important to indicate that calculated silica matrix refractive index, by EEP for various humidity, is n_{700} = 1.44 for pristine silica whereas for Na-SiO_2 (Na/Si = 0.5) inorganic matrix is n_{700} = 1.45. Without doubt, the measured increase of optical density of the silica skeleton is due to the insertion of sodium atoms, meaning that previous described drastic increases of refractive index are due to the combination of a densification process and an alkali ions insertion. Considering both phenomena, we estimate for Na-SiO_2 (Na/Si = 0.5) film

that refractive index change results for 94% from the silica matrix densification while the remnant 6% comes from the presence of sodium. This confirms that densification of the mesoporous Na-SiO_2 films is preponderant.

Second, additional increase of Na content above Na/Si = 0.5, promotes, after film washing, a slow decrease of refractive index, reaching n_{700} = 1.32 for the initial Na/Si molar ratio value of 2.1. In that range of composition, the contraction of films progressively decreases with the increase of the Na/Si ratios. A Na-SiO_2 film contraction of 36% is measured at Na/Si = 0.5, whereas it is only 22.5% for Na/Si = 2.1. Concerning porous volumes of Na-SiO_2 layers, values of 11% and 27% for Na/Si ratios of 0.5 and 2.1 have been determined respectively. It is still lower than pristine porous silica (48%). Nevertheless the densification tends to be clearly limited with the increase of sodium, which is counter-intuitive considering the sodium-fueled process of densification described for the first part of plots with low sodium contents. Interestingly, the cross section SEM image of Na-SiO_2 film obtained for an initial molar ratio Na/Si = 2.1 (Figure 1c) shows pores with sizes up to 35 nm in diameter, which is clearly larger than the initial pore sizes, around 2 nm, we measured for pristine CTAB-templated silica thin films. Such unexpected porosity evolution led us to further investigate pore structure of Na-SiO_2 films by environmental ellipsometry porosimetry and SEM. The water adsorption-desorption isotherms obtained by EEP, all exhibited the typical type IV isotherm corresponding to an interconnected mesoporous network (not shown) for Na-SiO_2 layers prepared with 0 ≤ Na/Si ≤ 1.35. Pore size distributions extracted from such isotherms were determined using modified-Kelvin equation and are displayed in Figure 2.[21] At higher sodium ratios (Na/Si > 1.35) EEP using water vapors as gas probe was no more adapted to assess porosity due to the large pores diameters, and was then substituted by cross-section SEM. Pore size distributions obtained by SEM images processing have been added to Figure 2 (triangle dots).

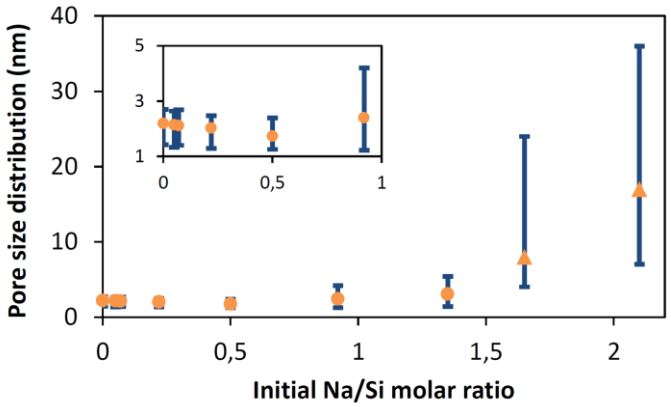

Figure 2. Pore size distribution (blue line) and mean pore size (orange dots) of Na-SiO_2 films depending on the initial molar ratio Na/Si obtained by EEP (round dots) using water vapors as gas probe for 0 ≤ Na/Si ≤ 1.35 and cross section SEM images processing (triangle dots) using ImageJ for Na/Si > 1.35. (inset) Zoom in on size distribution comprised between Na/Si = 0 and Na/Si = 0.92.

Pore size evolution depending on the initial Na/Si molar ratios, represented in Figure 2, exhibits here again two separated behaviors. In a first part, corresponding to the sodium range 0 ≤ Na/Si ≤ 0.5, we observed that porosity is mainly composed of pores centered around 2.2 nm in diameter at Na/Si = 0 and slightly decrease down to 1.7 nm for Na/Si = 0.5 (orange dots). Such reduction of pore sizes is in good agreement with the densification process previously concluded from the refractive indexes and thicknesses measurements. On contrary, the second part for Na/Si > 0.5 shows pore size distributions

that drastically and continuously widen with distributions (blue lines) comprised between (1.2 – 4.2 nm), (1.4 – 5.4 nm), (4 – 24 nm), and (7 – 36 nm), with mean diameters of 2.4 nm, 3.1 nm, 8 nm and 17 nm for initial Na/Si ratios of 0.9, 1.35, 1.65, and 2.1 respectively. The extensive increase of pore diameters observed by EEP and SEM confirms that densification process for Na-SiO_2 films synthesized with Na/Si > 0.5 is supplanted by another sodium ions-induced mechanism allowing the reconstruction of the initial 2 nm mesopores in larger mesopores.

1.2 Sodium ions assisted reconstruction mechanisms: Na_2O-SiO_2 phase diagram.

Both alkali ions assisted densification and alkali ions assisted reconstruction of mesoporous silica films are based on the ability of the alkali ionic species to modify the silica framework during their thermal diffusion and insertion in the siliceous network, and result in alkali-doped silica films or in other words, here, in sodium silicate thin films.

Amorphous sodium silicate has been the subject of many studies, especially in glass industry, and its structure modifications with Na_2O contents and temperature can be resumed using a Na_2O-SiO_2 phase diagram. Simulated, using commercial FactSage software, Na_2O-SiO_2 phase diagram is represented in Figure 3. It is characterized by the coexistence of two regions: (i) a region of compositions for which the sodium is miscible in silica and gives monophasic materials, and (ii) a second region of compositions for which the sodium is no more soluble, leading to a phase separation, and so to materials with two phases. The immiscibility region also called the immiscible dome (see Figure 3) is demarcated by a binodal curve, that contains three domains (two metastable and one unstable domains) separated by the spinodal curve. The metastable and unstable domains correspond to two distinct mechanisms of phase separation i.e. the nucleation and growth phase separation, and the spinodal decomposition.[41–44] Such Na_2O-SiO_2 phase diagram permits a better understanding of the relation between the sodium content in the silica matrix and the two observed reconstruction processes, as demonstrated in the following part.

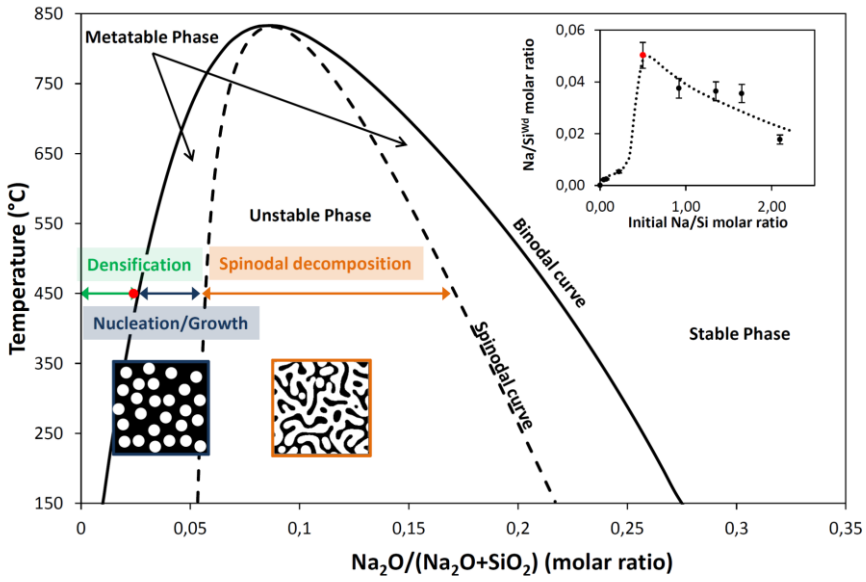

Figure 3. Simulated phase diagram (binodal curve) of amorphous Na_2O-SiO_2 solid solution using FactSage software. The spinodal curve has been added arbitrarily to complete the phase diagram. (inset) Plot of the Na/Si^{Wd} molar ratios in Na-SiO_2 films after washing, obtained by atomic adsorption spectroscopy depending on the initial Na/Si molar ratios. Red dots correspond to the composition of silica-rich phase formed during phase separation.

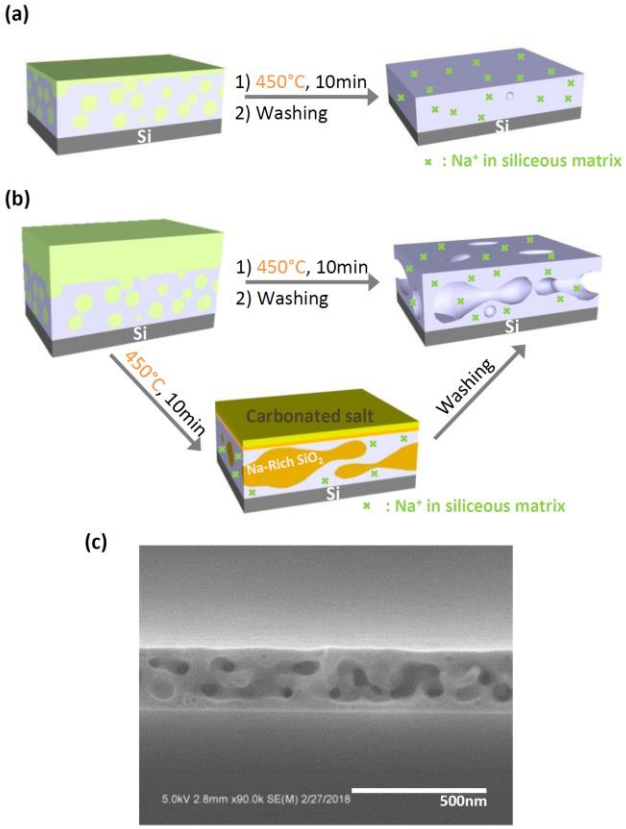

Figure 4. (a), (b) Illustrations of the densification and restructuration mechanisms of the Na-SiO_2 porous films for initial molar ratio Na/Si < 0.5 and Na/Si > 0.5 respectively. (c) Cross section SEM image of a Na-SiO_2 film obtained for an initial molar ratio Na/Si > 2.5.

For low content of sodium (0 < Na/Si < 0.5), we obtained Na-SiO_2 films showing porous volumes lower than the initial silica films due to the Na^+-assisted densification of the matrix. Indeed, as illustrated by the scheme in Figure 4.a, the thermal migration and insertion of Na^+ into the silica matrix at 450°C induces the breaking of Si-O-Si bonds to form sodium-silicate ionic bonds with an amount that increases with the Na/Si ratio. The lower degree of cross-liking in the SiO_2 framework is accompanied by a higher degree of mobility for tetrahedral SiO_4 units that can change their conformations in the film. In these conditions, micropores and mesopores elimination of the siliceous matrix is thermodynamically driven by the reduction of high energy interfaces which results in (1) the drastic diminution of the quantity of nanopores, (2) the diminution of the size of remaining pores and *in fine* (3) the densification of the silica films.

A quantitative investigation of Na^+ chemical activity as pore modifier was conducted in order to assess the real amount of sodium atoms that participates to the densification and reconstruction processes. Atomic adsorption spectroscopy (AAS) analyses of Na-SiO_2 layers after washing was performed, by dissolving them in 1 vol% HF solution, to determine the Na/Si^{Wd} molar ratios which correspond to the quantity of sodium ions entrapped in silica matrix after treatment. Results are reported in Figure 3 inset. We observed for low initial Na/Si ratios (Na/Si < 0.5) that partially densified porous silica matrixes retained a low quantity of Na^+, corresponding to less than 5% of the initial amounts spin coated on the pristine silica layers. It is likely that the spin coating of low concentrated sodium acetate solutions partially filled the mesopores with salt whereas a small

amount of salt covered the top surface of films. During annealing at 450°C, a small part of the sodium probably diffused in silica in equilibrium with the rest of the sodium turned into Na_2CO_3 by the thermal treatment.[45] The diffusing Na^+ participates to the densification whereas sodium carbonate is entrapped in silica matrix before being eliminated by the acidic washing. Both the decrease of refractive indexes during the washing step and the fact that the films thicknesses remain constant support this hypothesis. The abrupt increase of sodium content in silica observed for the film synthesized at initial Na/Si = 0.5 is linked to the maximum of the densification process described previously. Here, 10% of the initial Na^+ amount is sequestrated into the silica framework with a corresponding Na/Si^{Wd} = 0.05 (± 10%) ratio in the washed Na-SiO_2 layer. This ratio, measured at the acme of the densification process and just before the beginning of the pore reconstruction, correponds to the binodal curve at 450°C with a composition $Na_2O/(Na_2O+SiO_2)$ = 0.025 (marked with a red dot in the phase diagram in Figure 3). This indicates that densification process takes place at 450°C in the miscible region (marked by a green arrow) for Na_2O composition in silica comprised between 0% and 2.5%.

Since for an initial Na/Si = 0.5 the quantity of sodium ions diffusing in the silica films is equivalent to Na_2O molar ratio at the limit of the binodal curve (also called coexistence curve). Logically, **for higher content of sodium (Na/Si > 0.5)**, the quantity of sodium ions in silica films is susceptible to exceed the limit of solubility. Therefore, a phase separation driven by thermodynamic competition between enthalpy and entropy of the mixture can appear with the formation of one alkali-rich phase and one silica-rich phase.[41–44] Experimentally and as described in the illustration of pore reconstruction process in Figure 4b, phase separation generates a Na-rich phase that is soluble in water and can be washed simultaneously with the excess of salt using water at pH = 2. Na-rich phase elimination leaves a new porosity within the insoluble silica-rich matrix. According to initial Na/Si ratio, pore sizes go from 1.7 nm to 35 nm for Na/Si = 0.5 to 2.1 (Figure 2). But whatever the initial quantity of sodium used in this range, all pores exhibit a spherical morphology (see Figure 1c) that is typical of the nucleation/growth phase separation encountered in metastable domains of the phase diagram for Na_2O composition in silica superior to 0.025 (see Figure 3).
The quantitative assessment of Na^+ inserted in silica matrix after treatment, by AAS, for high initial Na/Si ratios (0.5 < Na/Si < 2.1) is reported in Figure 3 inset. It shows a continuous decrease of the sodium content entrapped in the insoluble silica-rich phase (Na/Si^{Wd}). Such an evolution is caused by a bias in the calculation method. Indeed, we consider that silica molar content in the layers after washing is similar to the one introduced with pristine layers before sodium treatment. Nonetheless this hypothesis is no more adapted in case of phase separation because the Na-rich phase elimination during the acidic washing also drags away silicate species. That's the reason why, we assume that sodium content in silica-rich phase after washing of Na-SiO_2 layers obtained with 0.5 < Na/Si < 2.1, must be equal to the one observed for a Na-SiO_2 film synthesized by an initial Na/Si = 0.5, i.e. Na/Si^{Wd} = 0.05 (red dot in Figure 3). Meaning at 450°C that the thermal insertion and chemical activity of around 5 Na^+ atoms in a 2 nm porous silica sol gel cluster of about 100 atoms of Si is enough to densify the siliceous structure. And that insertion of one more sodium ion is susceptible to trigger the phase separation of the mixture following a nucleation/growth mechanism.

For very **high contents of sodium (Na/Si > 2.5)**, as shown by the SEM cross section image reported in Figure 4c, the porous silica reconstruction by alkali ions provides Na-SiO_2 films with worm-like pores showing sizes over 100 nm. This disorganized large porosity probably results from the continuous

interpenetrating of the Na-rich and silica-rich phases, what is characteristic of spinodal decomposition. The Na_2O-SiO_2 metastable mixture obtained for 0.5 < Na/Si < 2.1 evolves towards a complete unstable state when the diffusing sodium amount in silica matrix increases over the spinodal curve composition, typically for Na/Si > 2.5 (see Figure 3). Location of porosity in the center of the layer seems to indicate that interfacial energies at the air interfaces is favored in case of silica-rich phase, which confines the water soluble Na-rich phase between a top silica-rich layer and a bottom silica layer generated by the alkali-induced oxidation of the silicon substrate, as demonstrated hereafter. One adds that for the highest quantity of sodium, because deposited salt layer is not perfectly homogeneous, some disseminated holes going through the coating are formed during the washing due to local extra rich sodium domains.

While the crucial role of sodium content was emphasized concerning pore size evolution, the importance of the annealing treatment in the process of thermal diffusion of the ions has also to be stressed. As reported in the Supplementary Information (S.I.3), variations of annealing time at 450°C induced significant changes in the reconstruction process, highlighted by an increase of films refractive indexes observed for all initial sodium contents. For instance, n_{700} = 1.37 and n_{700} = 1.48 are observed for annealing times of 5 min and 1h respectively in case of initial Na/Si = 0.5. Thickness measurements also show higher contraction of thin films for all sodium contents when annealing time increases. All these observations are characteristic of a global porous framework densification. It highlights that if porosity reconstruction is driven by thermodynamics, kinetics have to be considered due to the large material viscosities. Annealing time of 10 min at 450°C was determined as the best compromise to kinetically control the activity of sodium ions as porosity modifier.[42] Unexpectedly, alkali ions catalyzed thermal oxidation of silicon substrates, generating dense SiO_2 interstitial layers showing thickness up to c.a. 50 nm, have been observed for high initial Na/Si ratios and long annealing times, see S.I.3. Such oxidation of the silicon substrates is discussed more hereafter.

One also adds that sodium ions assisted porosity restructuration process was successfully extended to F127-templated mesoporous silica films with initial pore sizes of 8 nm. Refractive index and thickness plots of Na-SiO_2 films for 0 ≤ Na/Si ≤ 1.8 are reported in S.I.4 as well as cross section SEM images. We observed identical nanostructure evolution than the one observed for CTAB templated films with first a sodium assisted densification of films then a sodium assisted reconstruction process allowing the creation of large pores with sizes up to 25 nm. To go further, creation of a mesoporosity starting from xerogel silica films was attempted by sodium insertion. We observed for low sodium contents an increase of the refractive index of silica films from n_{700} = 1.41 to 1.46 attributed to the sodium insertion. Rapidly, for Na/Si ≥ 0.6, micrometer scale holes in the layers are formed and no mesopore is observed by ellipsometry or SEM. Therefore, it can be concluded that alkali ions assisted pore engineering is an efficient process of pore reconstruction but not a process of pore creation.

2) SiO_2 Mesopore Reconstruction Using Lithium or Potassium ions.

In the following part, the same investigations were conducted with lithium acetate and potassium acetate solutions as an alternative to the previous sodium acetate solutions, and also to clarify the role of alkaline metal ions. As previously observed with sodium, a significant mesostructure transformation of the silica films upon Li^+ and K^+ treatment is evidenced. The refractive index plots in Figure 5a show for both alkali ions a similar trend as in the case of Na^+, with first a strong augmentation of the refractive index for the low initial X/Si (X = Li or K) ratios then a slow continuous decrease when initial alkali ions contents increase. Film thicknesses evolutions presented in Figure 5b also report similar evolution for Li^+, Na^+ and K^+ with the abrupt films contraction in a first part before a more moderate thicknesses decrease at higher initial X/Si ratios. From these ellipsometry analyses, it's fairly clear that whatever the alkali ions, silica films undergo a densification as described previously for Na^+. However, it is also obvious, particularly from refractive index data, that such densification process is influenced by the type of ions with recorded utmost refractive index values of 1.38, 1.39, 1.40 obtained for initials K/Si = 0.3, Na/Si = 0.5 and Li/Si = 0.9 respectively.

Attending that films contraction for the three type of ions is almost equivalent, this maximums shift toward high ratio and high refractive index seems to point a discrepancy of alkali ion amounts in densified frameworks, with contents of $Li^+ > Na^+ > K^+$. To clarify this difference between the three alkali ions, quantification of Li^+, Na^+, K^+ ions inserted at 450°C into silica matrixes was performed by atomic absorption spectroscopy depending on initial X/Si (X = Li^+, Na^+, or K^+) ratios. Measurements were performed from solutions obtained by dissolving washed and dried thin films in 1 vol% HF solution. Results are reported in S.I.5. We observed that ratios of alkali ions caught in silica matrix of Li-SiO_2, Na-SiO_2 and K-SiO_2 densest films are significantly different with values: Li/Si^{Wd} = 0.13 (± 22%), Na/Si^{Wd} = 0.05 (± 10%), and K/Si^{Wd} = 0.03 (± 30%) while they all exhibit similar refractive indexes. It is important to remember that both silica matrix densification and insertion of alkaline metal ions contribute to the rise of films refractive index. However, given the low alkali contents monitored in these siliceous frameworks it is reasonable to assume that refractive index rises are mainly due to the loss of porosity. Recorded molar ratios therefore indicate that K^+ ions are more efficient than Na^+ to catalyze the densification process and much more than Li^+. As introduced previously, alkali ions assisted densification of mesoporous films is based on Si-O-Si bonds breaking by alkali ions to form ionic alkali-oxygen bonds that weaken the amorphous silica network. The increase of the number of nonbridging oxygen atoms enhances the conformational mobility of SiO_4 tetrahedra, allowing the reduction of the volume energy of the material. In same time, surface energy of the mobile silica framework is reduced by expulsion of the porosity. Ionic radii, ion mobility, and polarizability of alkali ions in the silica matrix are also important parameters that to be taking into account in this process. Indeed, thermal treatment at 450°C induced the Li^+, Na^+ and K^+ ion migration, with diffusion coefficients inversely proportional to the cation sizes (for example $D^{Li+} = 4.10^{-7}$ $cm^2.s^{-1}$, $D^{Na+} = 1.1.10^{-10}$ $cm^2.s^{-1}$, and $D^{K+} = 3.10^{-12}$ $cm^2.s^{-1}$ in glass at 350°C for ionic radii r^{Li+} = 0.6 Å, r^{Na+} = 1 Å, and r^{K+} = 1.4 Å respectively).[46,47] In other words, lithium ions are more susceptible to diffuse toward the nearest most constrained Si-O-Si bonds, which are the most reactive sites in the silica network, than Na^+ and K^+ ions.[48] However diffusion parameters are not the only ones to take into account. Indeed Mazzara et al. well described that creation of a nonbridging oxygen is accompanied by the rearrangement of silica tetrahedra surrounding the diffusing ion in a defined stereochemical order.[49] Highlighting that relaxation of amorphous silica network around the ion and *in fine* the film densification is the

combination of the creation of nonbridging oxygen atoms and also the steric effect of the diffusing cations. Because ionic volumes of $K^+ > Na^+ > Li^+$ and that number of oxygen atoms in silica network potentially affected by a cation increases when ions size increase, it is therefore reasonable to expect relaxation effects for $K^+ > Na^+ > Li^+$. What is in good agreement with the contractions and the AAS recorded alkali ions inserted in dense thin film after washing.

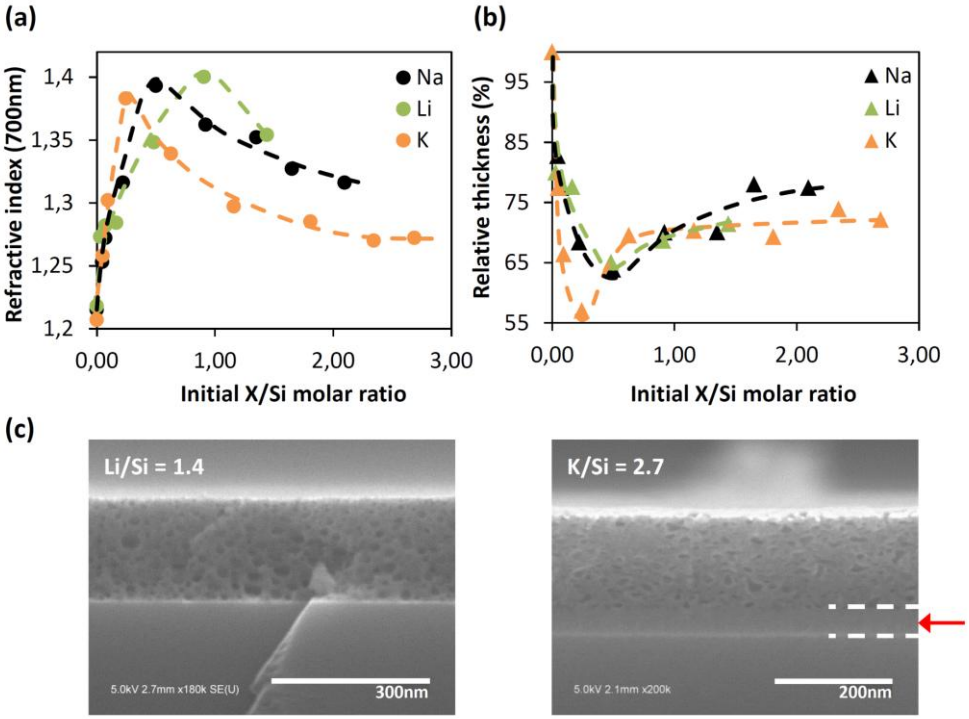

Figure 5. (a) Refractive index and (b) relative thickness of Li-SiO_2, K-SiO_2 and Na-SiO_2 films depending on the initial molar quantities of lithium acetate, potassium acetate and sodium acetate respectively. (c) Cross section SEM images of Li-SiO_2 (left) and K-SiO_2 (right) films obtained from initial molar ratios Li/Si = 1.4 and K/Si = 2.7.

As seen previously by using sodium ions, the porous silica film densification mechanism induced by diffusion of Li^+ and K^+ is followed by a phase separation process. Initial molar ratios from which the beginning of phase separation is observed are Li/Si ≥ 0.9, Na/Si ≥ 0.5 and K/Si ≥ 0.3. Such progressive shift toward high alkali concentration for K-SiO_2, Na-SiO_2 and Li-SiO_2 respectively is in excellent agreement with the immiscible dome position of corresponding K_2O-SiO_2, Na_2O-SiO_2 and Li_2O-SiO_2 phase diagrams (S.I.6). The SEM image shown in Figure 5c (left) corresponds to a Li-SiO_2 film synthesized with an initial Li/Si = 1.4. The pore size distribution ranges from 3 nm to 35 and pores show spherical shape illustrating, similarly to sodium-assisted reconstruction process, the generation of large pores by phase separation through a nucleation/growth mechanism.

In case of lithium-assisted porosity reconstruction, when initial Li/Si ≥ 1.4, optical microscopy and SEM characterizations of Li-SiO_2 films revealed many pores of several tens of micrometers in diameter that perforate the silica layers and prevent any optical characterization by ellipsometry (see S.I.7). Craters density increases with the initial quantity of lithium ions until an almost complete dissolution of the layer at Li/Si ≥ 2 during washing operations. Such microscopic scale holes have also been observed in Na-SiO_2 films for Na/Si > 2.1 but with a relative low surface density, while they have

never been observed for K-SiO_2 layers in the observed range that extend up to K/Si = 3. Such microscopic structures are revealed during the dissolution of cation-rich phase by the washing and result certainly from an intense nucleation/growth phase separation. Formation of these local and micrometer scale round-shape alkali-rich phases requires a large amount of diffusing cations in silica matrix. Because mobility of $Li^+ > Na^+ > K^+$, high concentration of alkali ions is probably attained first with relatively low initial Li/Si ratios then for higher Na/Si ratios and finally a probable much larger K/Si ratios.

Concerning potassium-assisted pore reconstruction, SEM image in Figure 5d (right) of K-SiO_2 film obtained for an initial K/Si = 2.7 also exhibit large pores (3 to 25 nm) resulting from the extraction of the aqueous soluble K-rich phase formed by the separation phase. The not well define shapes of pores observed in Figure 5d seems to point that at K/Si = 2.7, potassium silicate mixture is close to evolve from a nucleation/growth phase separation to a spinodal decomposition. Surprisingly, for high initial K/Si ≥ 0.6, an interstitial layer between the silicon substrate and the top porous K-SiO_2 film is observed (red arrow in Figure 5c). It is important to remark that only thickness and refractive index of porous layers are reported in Figure 5a and b. Ellipsometry and SEM investigations of K-SiO_2 films (S.I.8) as well as experiments consisting in the thermal annealing of potassium acetate onto bare silicon substrate revealed that this intermediate layer is a dense layer of SiO_2. This silica layer results from the oxidation of the silicon substrate during the thermal curing step of sample at 450°C for 10 min. We evidenced that higher the initial potassium amount and thicker is the SiO_2 layer for K/Si ratios comprised between 0.6 and 2.3. Over K/Si = 2.3, thickness of the interstitial SiO_2 layer seems to stabilize at around 40 nm (see S.I.8). In addition to play the role of porosity modifier of silica framework, at film-silicon substrate interface, alkali ions act as a catalyst for the thermal oxidation of the silicon substrate. Alkali metal ions favor the oxygen diffusion through the passivating native silica layer of silicon and enhanced oxidation of the underneath metal as previously reported by Revesz *et al.*.[50] No Li^+ induced oxidation of the silicon substrate have been evidenced at 450°C, whereas an oxide layer with a thickness of a ten of nanometer was observed for Na-SiO_2 films synthesized at Na/Si ≥ 1.5.

3) Patterned Nanostructured Materials: Antireflective Coating with a Gradient of Property.

Alkali ions assisted pore reconstruction is a straightforward, versatile, and low cost process to engineer pore sizes and porous fraction of silica films with potential in a broad range of applications. One of them concerns the systems with directional graded optical properties that have a promising potential in the development of optical adaptive devices such as Bragg reflectors, waveguides, antireflective coatings, *etc.* due to their ability to adapt, in real time, their response. Dip coating process in acceleration mode have recently been demonstrated as a powerful tool to synthesized sol gel multistacks with controlled gradient of optical and surface energy properties.[51] Here we demonstrate an alternative to fabricate one layer sol gel films with controlled gradient of optical property using sodium ions assisted reconstruction of mesoporous silica nanostructure. The optical system is prepared by the successive deposition onto a microscope glass substrate of a dense TiO_2 layer and a CTAB-mesoporous SiO_2 layer. Each layer was annealed at 450°C just after deposition. The refractive indexes were measured to be n_{700} = 2.1 for the crystalline TiO_2 sublayer and n_{700} = 1.22 for the SiO_2 top layer with the respective thicknesses of 140 nm and 125 nm. Here titania layer was selected as buffer layer in order to block the sodium diffusion from the soda lime glass substrate toward the silica film. Then, a hydro-alcoholic sodium acetate solution (6 $mg.ml^{-1}$) was sprayed, using an airbrush, onto the silica film. Spray and sample were placed in normal position of each other at a distance of around 30 cm (see schematic in Figure 6.a), with the edge of the film in front of the spray nozzle (spray angle position = 0°). Solution was sprayed for 1 min while the substrate was heated at 70°C to accelerate solvent evaporation. Then sample was treated at 450°C, washed with pH = 2 water, rinsed with water and dried.

Before assessing antireflective properties of the prepared optical system, refractive index of a spray-prepared Na-SiO_2 film was performed by ellipsometry, see Figure 6b. For the sake of simplicity, glass substrate has been replaced by silicon to avoid backside reflection and the ion blocking layer was removed. Refractive index recorded along the x axe going from the left to the right of the Na-SiO_2 film is plotted in Figure 6b as a function of the distance. A first gradient of refractive index is observed starting from n_{700} = 1.25 at x = 0 mm to 1.41 at the distance of 31 mm. This graded refractive index distribution results from the controlled sodium-induced densification of the porous silica. It follows a Gaussian like shape evolution imposed by the spray nozzle. Indeed, the airbrush spray generates a mist-type cone pattern that produces a Gaussian-like distribution of the sodium acetate solution resulting in a high sodium amount deposited in x = 31 mm and a low sodium content in x = 0 mm. The second gradient of refractive index over x = 31 mm, for the highest sodium concentration, corresponds to the phase separation driven reconstruction of the porous silica network accompanied by a decrease of refractive index from n_{700} = 1.41 to n_{700} = 1.33. Densification and phase separation phenomena previously observed on multiple samples for various quantity of sodium are gathered in a unique sample, illustrating that spray coating is a powerful technique to explore the isotherm of the Na_2O-SiO_2 phase diagram at 450°C. Combined with stencils, spray coating also allows preparing patterned surface. In Figure 6b (inset) a "PMC" pattern has been prepared by selective deposition of sodium acetate solution (6 $mg.ml^{-1}$). The letters exhibit a blue structural color due to the refractive index of n_{700} = 1.38 and the film thickness of 170 nm that results from the local densification of the yellow-colored mesoporous silica film that show a refractive index of n_{700} = 1.26 and a thickness of 230 nm.

Coming back to the glass coated with the antireflective layer (AR). Antireflective property of the Na-SiO_2 layer was assessed for various x positions, by comparing the transmittance in the visible range of the bare glass substrate and the one side coated glass. It must be clarified here that TiO_2 blocking layer also contributes to the antireflective property, however thickness and refractive index of the titania layer were monitored and show constant values all over the sample. Therefore any transmittance variations will be considered as only induced by the Na-SiO_2 layer. Transmittance curves recorded at RH ≈ 0% are presented in Figure 6c. A maximum of transmittance at around λ = 530 nm, common for all plots, is observed whatever the probed position of the AR. More interestingly a second maximum of transmittance at around λ = 800 nm can be modulated in intensity between 90% and 94% (Figure 6c inset) by moving the sample in front of the incident beam light in a range of 20 mm, which corresponds to a local refractive index variations of n_{700} = 1.28 at x = 0 mm to n_{700} = 1.41 at x = 20 mm. Modulation of the intensity of the second local maximum of transmittance allows to adapt the AR response from an almost perfect single wavelength AR to a broad band AR. Such optical system with graded AR property is particularly useful, in addition to theoretical simulation, to investigate rapidly the optical properties of a device as AR efficiency, structural colors, etc. without multiplying the samples.

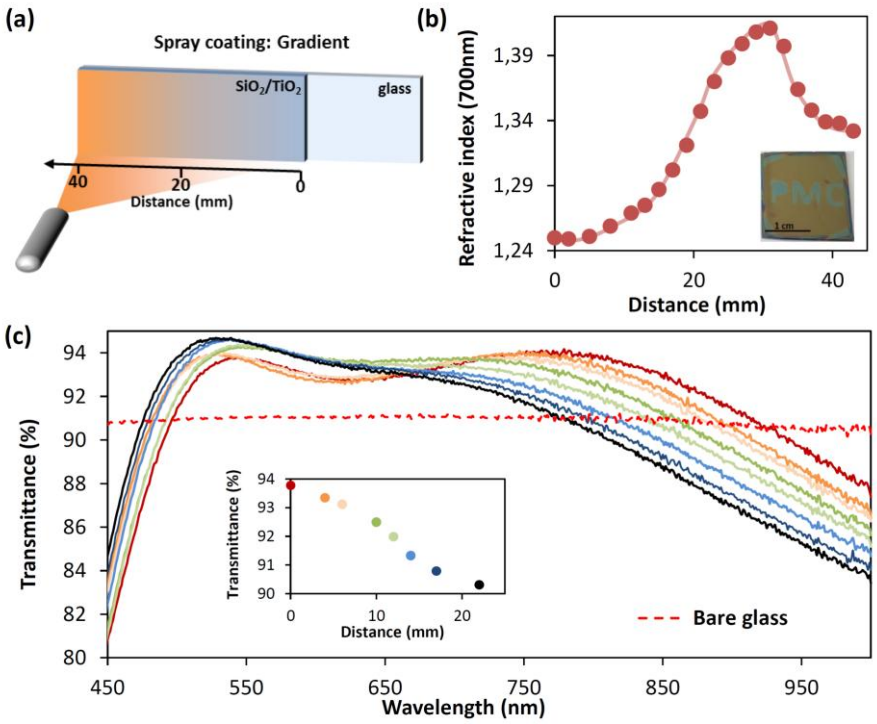

Figure 6. (a) Illustration of the process of spray coating to deposit sodium acetate film with a gradient of quantity onto a bilayer stack composed of a dense TiO_2 layer and a mesoporous SiO_2 layer. (b) Evolution of the refractive index at 700nm of the graded Na-SiO_2 layer along the x axe after washing. (inset) Picture of a CTAB-templated mesoporous silica layer patterned by spray coating using a "PMC" stencil. (c) Evolution of the antireflective property of the bilayers stack composed of dense TiO_2 and mesoporous Na-SiO_2 layers on glass substrate along the x axe, spectrophotometric measurements are performed in dry atmosphere.

A last investigation consisted in dissolution tests by immersing separately a pristine porous silica film, a partially densified Na-SiO_2 film synthesized at Na/Si = 0.07, an almost fully densified Na-SiO_2 film obtained at Na/Si = 0.5 and a porous Na-SiO_2 film restructured by phase separation which has been synthesized at Na/Si = 1.35 into 100 mL of aqueous pH 7.6 phosphate buffer solutions at 70°C. Such

accelerated environmental aqueous attack simulation aims to determine the influence of the low alkali ions amounts entrapped in siliceous matrixes on the film stability in water. Thickness evolution measured by ellipsometry before immersion and after various soaking times is performed to monitor the silica dissolution in water. Figure 7a gathers the obtained thickness evolutions. In general, Na-SiO_2 films show a higher stability in PBS solution than pristine porous silica films whatever the initial Na/Si ratio. Indicating that preponderant parameter influencing the films stability is their porous volumes. Indeed the almost fully densified Na-SiO_2 sample (Na/Si = 0.5) exhibits an excellent resistance toward aqueous dissolution because, compared to the others films. Because the surface area of the silica matrix is minimized, with a relative low porous fraction of 11%, the silica-water interfaces susceptible to be eroded by dissolution is limited. In order to assess only the chemical resistance of layers we reproduced the same experiments by comparing a Na-SiO_2 film obtained at Na/Si = 0.5 with a silica xerogel synthesized without any surfactant. They both possessed similar thicknesses and refractive indexes (n_{700} = 1.40 and h = 175 nm for Na/Si = 0.5 / n_{700} = 1.40 and h = 155 nm for the xerogel) as well as fairly similar porous volume of 9% and 6% respectively. In figure 7b thickness evolution for both samples are reported as a function of the time of immersion in PBS solution. We observe, after 4 h in PBS solution, that silica film restructured by sodium ions is totally dissolved in buffer solution whereas 75% of the xerogel film is still intact on the top of the silicon substrate. Experiments indicate that the sequestrated Na^+ in silica, inserted as a counter ions of non-bridging oxygen, effectively weaken the siliceous network but that general layers stability is a balance between porous volume of the material and its hydrolytic resistance.

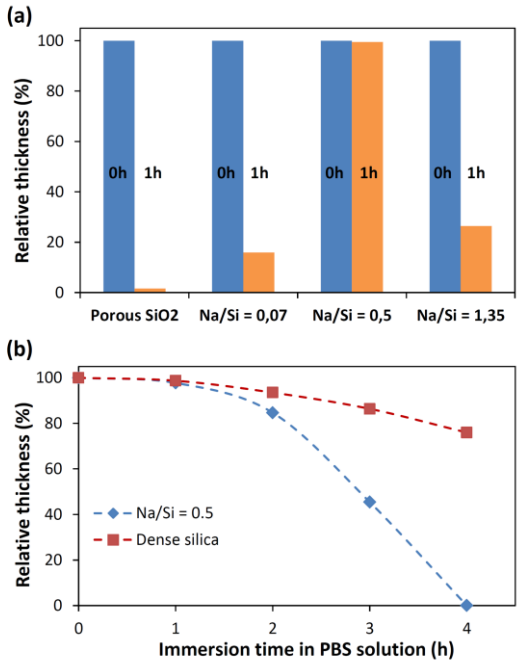

Figure 7. (a) Relative thickness reduction of porous CTAB-templated silica film, Na/Si = 0.07, Na/Si = 0.5, and Na/Si = 1.35 Na-SiO_2 films on silicon substrates after 0 h and 1 h of immersion in phosphate buffered saline solution at pH = 7.6. (b) Thickness reduction of sol gel dense silica layer (dense silica layer is prepared with a solution similar than CTAB-templated silica solution without surfactant) and Na/Si = 0.5 depending on the immersion time in phosphate buffered saline solution at pH = 7.6.

Hydrophobic post-functionalization with alkylsilanes or fluoroalkylsilanes of surface samples can be envisaged to improve water stability of alkali-reconstructed silica film.[52] Hybrid methylated silica networks were also reported as having a good resistance in water.[11] Nevertheless sodium ions-assisted reconstruction of such films is particularly difficult due to their strong hydrophobic surfaces and the ionic nature of hydro-alcoholic alkali metal solution that prevent homogeneous liquid deposition and required to adapt a new process.

Conclusion:

We have demonstrated that the alkali ions Li^+, Na^+ or K^+ diffusing under controlled conditions of temperature and concentration into mesoporous silica thin films act as nanostructure modifiers to selectively tailor both the porous volume and the pore sizes. Indeed, insertion of a low amount of alkali metal ions in silica was shown to decrease porous volume of films by a densification mechanism that involved relaxation of siliceous network through the creation of non-bridging oxygen atoms by breaking Si-O bonds and steric effect of inserted alkali ions itself. Controlled porous volume reduction up to 80% of the initial value has been demonstrated. Among studied alkali ions, K^+ exhibits a higher densification activity than Na^+ and Li^+. When quantity of alkaline metal ions in porous silica network increase, there is a composition for which the diffusing species are no more miscible, provoking a phase separation by segregating a silica-rich phase and an alkali-rich phase. Using Li^+, Na^+ or K^+ as pore modifiers, first a nucleation/growth type phase separation is obtained, generating the creation of spherical pores with sizes up to 35 nm. Then, still increasing ions quantity, dissolution of the silica film is observed during the process with Li^+ whereas Na^+ and K^+ allow observing the transition between nucleation/growth and spinodal decomposition resulting in very large pores with sizes up to 100 nm for Na-SiO_2 films.

In addition to be straightforward, this synthesis route involved a low number of steps, low cost acetate reagents and industrial routine techniques favorable for scale up. The successful demonstration of alkali ions assisted reconstruction of 2 nm (CTAB) and 7 nm (F127) mesoporous silica films allows glimpsing infinite number of porous nanostructure by combining different bare mesoporous silica film and alkali ions as pore modifier. Finally this process is particularly interesting to synthesize porous film with patterned structure. One example is the fabrication of glass an antireflective layer with a gradient of porous volume showing a high performance single wavelength AR property that can progressively turns into a broad band AR by shifting the optical device along the refractive index gradient axe of the coating. Finally alkali ions assisted pore restructuration is a new tool that can be added to the sol gel chemist's bottom-up and top-down techniques toolbox for the on-demand fabrication of meso-, micro- and macro-structured materials.

Associated Content:

Supporting information.

- Environmental porosimetry ellipsometry characterization of the mesoporosity of pristine CTAB-templated silica thin films.
- Drawing of the process of alkali ions insertion in mesoporous silica films.
- Spectroscopic ellipsometry and SEM characterizations of the refractive indexes and thicknesses of Na-SiO2 films synthesized with initial Na/Si = 0.07, Na/Si = 0.5, and Na/Si = 1.3 at 450°C for various annealing time.

- Spectroscopic ellipsometry and SEM characterizations of the refractive indexes, thicknesses and porosities of Na-SiO2 films synthesized from F127 templated silica films depending on the initial Na/Si molar ratio.
- Atomic absorption spectroscopy quantification of Li+, Na+, K+ ions inserted into silica matrixes after thermal diffusion, washing and drying.
- Simulated phase diagrams of amorphous Na2O-SiO2 / Li2O-SiO2 / K2O-SiO2 solid solutions using FactSage Software.
- Optical microscopy and SEM characterizations of Li-SiO2 films synthesized with initial molar ratio Li/Si ≥ 1.4.
- Spectroscopic ellipsometry and SEM characterizations of the potassium-catalyzed interstitial silicon oxide layers formed at 450°C for 10min during K-SiO2 films synthesis depending on the initial K/Si molar ratio.

This material is available free of charge via the Internet at http://pubs.acs.org/.

Author Information:

Corresponding Authors

-Email: mickael.boudot@polytechnique.edu, thierry.gacoin@polytechnique.edu

Notes

The authors declare no competing financial interest.

Acknowledgments:

The authors sincerely thank Dr. Sandrine Tusseau-Nenez for GIXRD experiments, as well as Pr. Yves Mechulam for its help for the atomic absorption spectroscopy analyses.

References:

(1) Sanchez, C.; Boissière, C.; Grosso, D.; Laberty, C.; Nicole, L. Design, Synthesis, and Properties of Inorganic and Hybrid Thin Films Having Periodically Organized Nanoporosity †. *Chem. Mater.* **2008**, *20*, 682–737.

(2) Faustini, M.; Boissière, C.; Nicole, L.; Grosso, D. From Chemical Solutions to Inorganic Nanostructured Materials: A Journey into Evaporation-Driven Processes. *Chem. Mater.* **2014**, *26*, 709–723.

(3) Sanchez, C.; Belleville, P.; Popall, M.; Nicole, L. Applications of Advanced Hybrid Organic-Inorganic Nanomaterials: From Laboratory to Market. *Chem. Soc. Rev.* **2011**, *40*, 696–753.

(4) C.J. Brinker and G.W. Scherer. *Sol Gel Science: The Physics and Chemistry of Sol-Gel Processing*; Academic Press, NY, 1990.

(5) Evans, D. F.; Wennerström, H. *The Colloidal Domain: Where Physics, Chemistry, Biology, and Technology Meet, 2nd Edition*; Wiley-VCH, 1999.

(6) Israëlachvili, J. *Intermolecular and Surface Forces*; 3rd Editio.; Academic Press, NY, 2011.

(7) Taguchi, A.; Schüth, F. *Ordered Mesoporous Materials in Catalysis*; 2005; Vol. 77.

(8) Townson, J. L.; Lin, Y.; Agola, J. O.; Carnes, E. C.; Leong, H. S.; Lewis, J. D.; Haynes, C. L.; Brinker, C. J. Re-Examining the Size/Charge Paradigm: Differing in Vivo Characteristics of Size- and Charge-Matched Mesoporous Silica Nanoparticles. *J. Am. Chem. Soc.* **2013**, *135*, 16030–16033.

(9) Boudot, M.; Elettro, H.; Grosso, D. Converting Water Adsorption and Capillary Condensation in Usable Forces with Simple Porous Inorganic Thin Films. *ACS Nano* **2016**, *10*, 10031–10040.

(10) Van Opdenbosch, D.; Fritz-Popovski, G.; Wagermaier, W.; Paris, O.; Zollfrank, C. Moisture-Driven Ceramic Bilayer Actuators from a Biotemplating Approach. *Adv. Mater.* **2016**, *28*,

5235–5240.

(11) Boudot, M.; Gaud, V.; Louarn, M.; Selmane, M.; Grosso, D. Sol–Gel Based Hydrophobic Antireflective Coatings on Organic Substrates: A Detailed Investigation of Ammonia Vapor Treatment (AVT). *Chem. Mater.* **2014**, *26*, 1822–1833.

(12) Wagner, T.; Haffer, S.; Weinberger, C.; Klaus, D.; Tiemann, M. Mesoporous Materials as Gas Sensors. *Chem. Soc. Rev.* **2013**, *42*, 4036–4053.

(13) Du, X.; Kleitz, F.; Li, X.; Huang, H.; Zhang, X.; Qiao, S.-Z. Disulfide-Bridged Organosilica Frameworks: Designed, Synthesis, Redox-Triggered Biodegradation, and Nanobiomedical Applications. *Adv. Funct. Mater.* **2018**, *28*, 1707325.

(14) Boissiere, C.; Grosso, D.; Lepoutre, S.; Nicole, L.; Bruneau, A. B.; Sanchez, C. Porosity and Mechanical Properties of Mesoporous Thin Films Assessed by Environmental Ellipsometric Porosimetry. *Langmuir* **2005**, *21*, 12362–12371.

(15) Zhao, D.; Yang, P.; Melosh, N.; Feng, J.; Chmelka, B. F.; Stucky, G. D. Continuous Mesoporous Silica Films with Highly Ordered Large Pore Structures. *Adv. Mater.* **1998**, *10*, 1380–1385.

(16) Innocenzi, P.; Malfatti, L.; Soler-Illia, G. J. A. A. Hierarchical Mesoporous Films: From Self-Assembly to Porosity with Different Length Scales. *Chem. Mater.* **2011**, *23*, 2501–2509.

(17) Sel, O.; Kuang, D.; Thommes, M.; Smarsly, B. Principles of Hierarchical Meso- and Macropore Architectures by Liquid Crystalline and Polymer Colloid Templating. *Langmuir* **2006**, *22*, 2311–2322.

(18) Yang, X.-Y.; Chen, L.-H.; Li, Y.; Rooke, J. C.; Sanchez, C.; Su, B.-L. Hierarchically Porous Materials: Synthesis Strategies and Structure Design. *Chem. Soc. Rev.* **2017**, *46*, 481–558.

(19) Sun, M. H.; Huang, S. Z.; Chen, L. H.; Li, Y.; Yang, X. Y.; Yuan, Z. Y.; Su, B. L. Applications of Hierarchically Structured Porous Materials from Energy Storage and Conversion, Catalysis, Photocatalysis, Adsorption, Separation, and Sensing to Biomedicine. *Chem. Soc. Rev.* **2016**, *45*, 3479–3563.

(20) Gao, F.; Botella, P.; Corma, A.; Blesa, J.; Dong, L. Monodispersed Mesoporous Silica Nanoparticles with Very Large Pores for Enhanced Adsorption and Release of DNA. *J. Phys. Chem. B* **2009**, *113*, 1796–1804.

(21) Boudot, M.; Ceratti, D. R.; Faustini, M.; Boissière, C.; Grosso, D. Alcohol-Assisted Water Condensation and Stabilization into Hydrophobic Mesoporosity. *J. Phys. Chem. C* **2014**, *118*, 23907–23917.

(22) Ashley, C. E.; Carnes, E. C.; Epler, K. E.; Padilla, D. P.; Phillips, G. K.; Castillo, R. E.; Wilkinson, D. C.; Wilkinson, B. S.; Burgard, C. a; Kalinich, R. M.; *et al.* Delivery of Small Interfering RNA by Peptide-Targeted Mesoporous Silica Nanoparticle-Supported Lipid Bilayers. *ACS Nano* **2012**, *6*, 2174–2188.

(23) Kim, M. H.; Na, H. K.; Kim, Y. K.; Ryoo, S. R.; Cho, H. S.; Lee, K. E.; Jeon, H.; Ryoo, R.; Min, D. H. Facile Synthesis of Monodispersed Mesoporous Silica Nanoparticles with Ultralarge Pores and Their Application in Gene Delivery. *ACS Nano* **2011**, *5*, 3568–3576.

(24) Schmidt-Winkel, P.; Lukens, W. W.; Zhao, D.; Yang, P.; Chmelka, B. F.; Stucky, G. D. Mesocellular Siliceous Foams with Uniformly Sized Cells and Windows. *J. Am. Chem. Soc.* **1999**, *121*, 254–255.

(25) Ogawa, M. Preparation of Layered Silica−Dialkyldimethylammonium Bromide Nanocomposites. *Langmuir* **1997**, *13*, 1853–1855.

(26) Brinker, C. J.; Lu, Y.; Sellinger, A.; Fan, H. Evaporation-Induced Self-Assembly: Nanostructures Made Easy. *Adv. Mater.* **1999**, *11*, 579–585.

(27) Dunphy, D. R.; Sheth, P. H.; Garcia, F. L.; Brinker, C. J. Enlarged Pore Size in Mesoporous Silica Films Templated by Pluronic F127: Use of Poloxamer Mixtures and Increased template/SiO2 Ratios in Materials Synthesized by Evaporation-Induced Self-Assembly. *Chem. Mater.* **2015**, *27*, 75–84.

(28) Deng, Y.; Yu, T.; Wan, Y.; Shi, Y.; Meng, Y.; Gu, D.; Zhang, L.; Huang, Y.; Liu, C.; Wu, X.; *et al.* Ordered Mesoporous Silicas and Carbons with Large Accessible Pores Templated from Amphiphilic Diblock Copolymer Poly(ethylene Oxide)-B-Polystyrene. *J. Am. Chem. Soc.* **2007**, *129*, 1690–1697.

(29) Nisticò, R.; Scalarone, D.; Magnacca, G. Sol-Gel Chemistry, Templating and Spin-Coating Deposition: A Combined Approach to Control in a Simple Way the Porosity of Inorganic Thin Films/coatings. *Microporous Mesoporous Mater.* **2017**, *248*, 18–29.

(30) Yu, K.; Smarsly, B.; Brinker, C. J. Self-Assembly and Characterization of Mesostructured Silica Films with a 3D Arrangement of Isolated Spherical Mesopores. *Adv. Funct. Mater.* **2003**, *13*, 47–52.

(31) Guillemot, F.; Brunet-Bruneau, a.; Bourgeat-Lami, E.; Gacoin, T.; Barthel, E.; Boilot, J.-P. Latex-Templated Silica Films: Tailoring Porosity to Get a Stable Low-Refractive Index. *Chem. Mater.* **2010**, *22*, 2822–2828.

(32) Nemanashi, M.; Noh, J.-H.; Meijboom, R. Dendrimers as Alternative Templates and Pore-Directing Agents for the Synthesis of Micro- and Mesoporous Materials. *J. Mater. Sci.* **2018**, *53*, 12663–12678.

(33) Malfatti, L.; Falcaro, P.; Marongiu, D.; Casula, M. F.; Amenitsch, H.; Innocenzi, P. Self-Assembly of Shape Controlled Hierarchical Porous Thin Films: Mesopores and Nanoboxes. *Chem. Mater.* **2009**, *21*, 4846–4850.

(34) Miao, X.; Sun, D. Graded/gradient Porous Biomaterials. *Materials (Basel).* **2010**, *3*, 26–47.

(35) Hor, J. L.; Jiang, Y.; Ring, D. J.; Riggleman, R. A.; Turner, K. T.; Lee, D. Nanoporous Polymer-Infiltrated Nanoparticle Films with Uniform or Graded Porosity via Undersaturated Capillary Rise Infiltration. *ACS Nano* **2017**, *11*, 3229–3236.

(36) Drisko, G. L.; Carretero-Genevrier, A.; Gich, M.; Gàzquez, J.; Ferrah, D.; Grosso, D.; Boissière, C.; Rodriguez-Carvajal, J.; Sanchez, C. Water-Induced Phase Separation Forming Macrostructured Epitaxial Quartz Films on Silicon. *Adv. Funct. Mater.* **2014**, *24*, 5494–5502.

(37) Niklasson, G. a; Granqvist, C. G.; Hunderi, O. Effective Medium Models for the Optical Properties of Inhomogeneous Materials. *Appl. Opt.* **1981**, *20*, 26–30.

(38) Innocenzi, P.; Malfatti, L.; Kidchob, T.; Costacurta, S.; Falcaro, P.; Marmiroli, B.; Cacho-Nerin, F.; Amenitsch, H. Densification of Sol-Gel Silica Thin Films Induced by Hard X-Rays Generated by Synchrotron Radiation. *J. Synchrotron Radiat.* **2011**, *18*, 280–286.

(39) Yoldas, B. E. Deposition and Properties of Optical Oxide Coatings from Polymerized Solutions. *Appl. Opt.* **1982**, *21*, 2960.

(40) Faustini, M.; Grenier, A.; Naudin, G.; Li, R.; Grosso, D. Ultraporous Nanocrystalline TiO 2 - Based Films: Synthesis, Patterning and Application as Anti-Reflective, Self-Cleaning, Superhydrophilic Coatings. *Nanoscale* **2015**, *7*, 19419–19425.

(41) Hodroj, A.; Simon, P.; Florian, P.; Chopinet, M. H.; Vaills, Y. Phase Separation and Spatial Morphology in Sodium Silicate Glasses by AFM, Light Scattering and NMR. *J. Am. Ceram. Soc.* **2013**, *96*, 2454–2460.

(42) Kreidl, N. Phase Separation in Glasses. *J. Non. Cryst. Solids* **1991**, *129*, 1–11.

(43) James, P. F. Liquid-Phase Separation in Glass-Forming Systems. *J. Mater. Sci.* **1975**, *10*, 1802–1825.

(44) HALLER, W.; BLACKBURN, D. H.; SIMMONS, J. H. Miscibility Gaps in Alkali-Silicate Binaries—Data and Thermodynamic Interpretation. *J. Am. Ceram. Soc.* **1974**, *57*, 120–126.

(45) Judd, M. D.; Plunkett, B. A.; Pope, M. I. The Thermal Decomposition of Calcium, Sodium, Silver and copper(II) Acetates. *J. Therm. Anal.* **1974**, *6*, 555–563.

(46) Stern, K. H. Glass-Molten Salt Interactions. *Chem. Rev.* **1966**, *66*, 355–372.

(47) Shannon, R. D. Revised Effective Ionic Radii and Systematic Studies of Interatomic Distances in Halides and Chalcogenides. *Acta Crystallogr. Sect. A* **1976**, *32*, 751–767.

(48) Rarivomanantsoa, M.; Jund, P.; Jullien, R. Sodium Diffusion through Amorphous Silica Surfaces: A Molecular Dynamics Study. *J. Chem. Phys.* **2004**, *120*, 4915–4920.

(49) Mazzara, C.; Jupille, J.; Flank, A.-M.; Lagarde, P. Stereochemical Order around Sodium in Amorphous Silica. *J. Phys. Chem. B* **2000**, *104*, 3438–3445.

(50) Revesz, A. G.; Evans, R. J. Kinetics and Mechanism of Thermal Oxidation of Silicon with Special Emphasis on Impurity Effects. *J. Phys. Chem. Solids* **1969**, *30*, 551–564.

(51) Faustini, M.; Ceratti, D. R.; Louis, B.; Boudot, M.; Albouy, P.-A.; Boissière, C.; Grosso, D. Engineering Functionality Gradients by Dip Coating Process in Acceleration Mode. *ACS Appl. Mater. Interfaces* **2014**, *6*, 17102–17110.

(52) Li, X.-M.; Reinhoudt, D.; Crego-Calama, M. What Do We Need for a Superhydrophobic Surface? A Review on the Recent Progress in the Preparation of Superhydrophobic Surfaces. *Chem. Soc. Rev.* **2007**, *36*, 1350–1368.

Table of Contents